Design of a Bi-Pulse Fiber Laser for Particle Image Velocimetry Applications

Driss Mgharaz[1], Marc Brunel[*,1] and Abdelkader Boulezhar[2]

[1]*UMR 6614 Coria CNRS UMR 6614, Avenue de l'Université, BP 12, 76801 Saint-Etienne du Rouvray Cedex, France*

[2]*Université Hassan II Ain Chock, B.P. 5366 Maarif, Casablanca 20100, Morocco*

Abstract: This paper presents the theoretical design of a Q-switched fiber laser, that can generate a pair of nanosecond microjoule pulses. Such a low-cost, compact, bi-pulse fiber laser would provide a very interesting alternative to classical PIV lasers.

1 - INTRODUCTION

Particle Image Velocimetry (PIV) or Digital PIV have important applications in flow measurements and spray characterization [1, 2]. PIV is an optical method used to obtain instantaneous velocity measurements and related properties in fluids. The fluid is seeded with tracer particles which are generally assumed to faithfully follow the flow dynamics. It is the motion of these seeding particles that is used to calculate velocity information of the flow being studied. PIV requires the emission of two nanosecond pulses, whose energies exceed the microjoule, while the separation between the two pulses must be more than 500 ns. This last limitation is due to the acquisition time of standard cameras classically used in PIV experiments.

The bi-pulse lasers classically used are Nd:YAG systems composed of two separate cavities. A synchronization system between them allows to adjust the delay between the pulses emitted by both cavities. The two pulses emitted are finally spatially superposed at the output of the system. Unfortunately, as both pulses are emitted by different cavities, the alignment suffers some imprecision which can become a limiting factor in the case of PIV applications with thin laser sheets. High power fiber lasers offer a very interesting alternative to Nd:YAG lasers. They are very compact and less expensive. They can operate either in Q-switched, mode-locked [3] or harmonic mode-locked regimes [4]. In addition, much progress has been observed in the last decade concerning the development of high power fiber lasers, and the emission of microjoule nanosecond pulses is not a problem. Finally, the emission of multipeak pulses has been evidenced recently [5], and it seems possible to emit a pair of pulses using only one fiber laser cavity. Such a device would significantly improve the precision in PIV experiments, as the spatial alignment of the two pulses would be systematically realized. We present in this paper the design of a fiber laser cavity that is able to emit a pair of pulses separated by more than 500 ns. The energy per pulse exceeds the microjoule and such a laser would satisfy PIV requirements. Section 2 presents the model developed. Section 3 presents the simulations obtained while section 4 shows the design of a cavity for PIV applications.

*Address correspondence to this author at the UMR 6614 Coria CNRS UMR 6614, Avenue de l'Université, BP 12, 76801 Saint-Etienne du Rouvray Cedex, France; E-mail: marc.brunel@coria.fr

2 - THEORETICAL MODEL

2.1. Configuration

The fiber laser that will be considered is based on the typical linear cavity described schematically in Fig. (**1**) [5]. The laser cavity consists of a laser medium (an Yb-doped double-clad fiber, noted YDF), an undoped fiber (a dispersion-shifted single-mode fiber, noted DSF) spliced on the right-hand side of the amplifying fiber [3, 6], an acousto-optic modulator and two mirrors of reflectivities R_1 and R_2. The pump power is injected on the left-hand side of the cavity through dichroïc mirror. The acousto-optic modulator (AOM) is positioned on the right-hand side of the cavity. The fibers are much longer than the other parts of the traveling path: the length of the other parts (L_R) is therefore neglected. The AOM is operating at its first diffraction-order. A right mirror is used to reflect the first-order beam back to the fiber core. The fiber has a core diameter of 16 μm, a numerical aperture of 0.06, and a first (inner) cladding with 400 μm, with a numerical aperture of 0.08. The numerical aperture of the fiber is relatively low (0.06-0.08) to support the single-mode transmission at the signal wavelength. We can thus neglect the difference between the core and the cladding indices.

2.2. Rate Equations

The modeling of Q-switched lasers can be categorized into the so-called ''point model'' [7, 8] and ''traveling-wave model'' [9, 10]. The former one is based on the assumption of a uniform gain distribution along the whole length of the laser cavity, which is obviously inappropriate for high-power fiber lasers, where the length of an active medium usually ranges from 5 to 30 meters. In traveling-wave model we assume that gain and intensity of radiation inside the laser cavity change as a function of the fiber length. Such an approach makes it possible to describe Q-switched fiber lasers precisely. The traveling-wave method requires relatively more complicated numerical procedure. It has been applied to different pulsed solid-state lasers and amplifiers, and led to great success in explanations of experimental

1874-3285/09

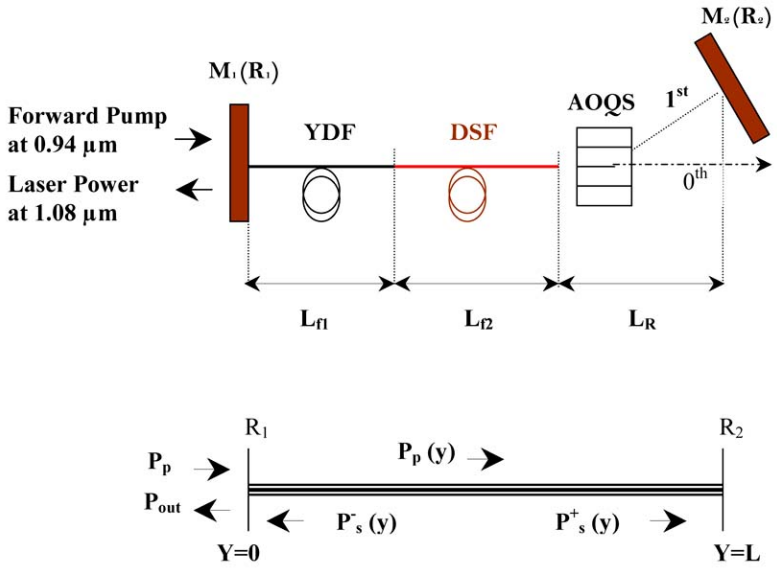

Fig. (1). (**a**) Design of our laser cavity. (**b**) Schematic illustration of the fiber laser geometry. $P_p(y)$ and P_{out} are respectively the pump and output powers, $P_s^+(y)$ and $P_s^-(y)$ are the signal powers propagating in the positive and negative y-direction respectively.

observations, and optimization of systems [10, 11]. In this work, we use this method to predict the switching dynamics of our Q-switched fiber laser.

The behavior of the Yb-doped double-clad fiber is described by the two-level pumping scheme shown in Fig. (**2**). $N_a(y,t)$ and $N_b(y,t)$ are the ground- and upper-level population densities, respectively, which are functions of time t and longitudinal position y in the Yb-doped fiber. The pump and signal light powers are represented by $P_p(y,t)$ and $P_s^{\pm}(y,t)$, respectively, which are functions of position and time. $\pm$ correspond to forward and backward components of the signal respectively. The equations that govern this system are detailed in the appendix.

2.2. Boundary Conditions

The equations detailed in the appendix are to be solved subject to the suitable boundary conditions imposed by the pumping scheme and the reflectors. They write:

$$P_p(0,t) = W_0$$

$$P_s^+(0,t) = R_1 P_s^-(0,t)$$

$$P_s^-(L,t) = R_2(t) P_s^+(L,t)$$

where W_0 is the pumping power. R_1 is the power reflectivity of the left reflector (at $y = 0$). The power reflectivity R_2 of the right mirror is modulated using the AOM as shown in Fig. (**3**), where T is the pulse repetition interval, τ_0 is the

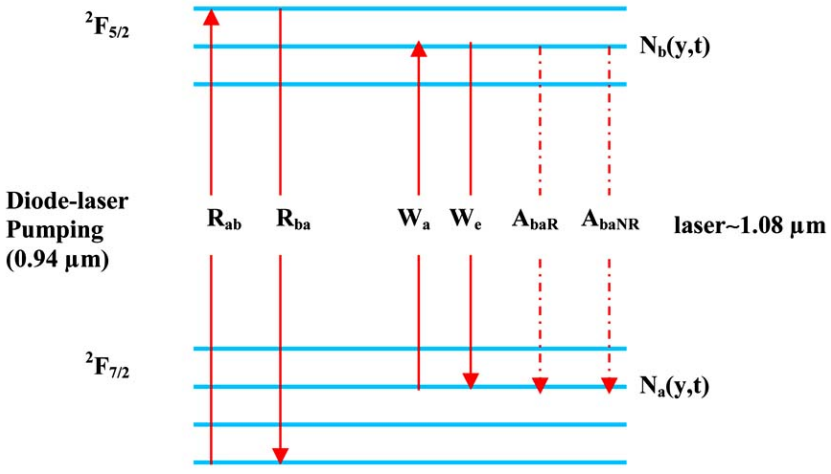

Fig. (2). Energy levels of Yb^{3+} ions, and the usual pump and laser transitions.

switching open time, and τ_r is the rise time. We approximate this modulation by the following expression:

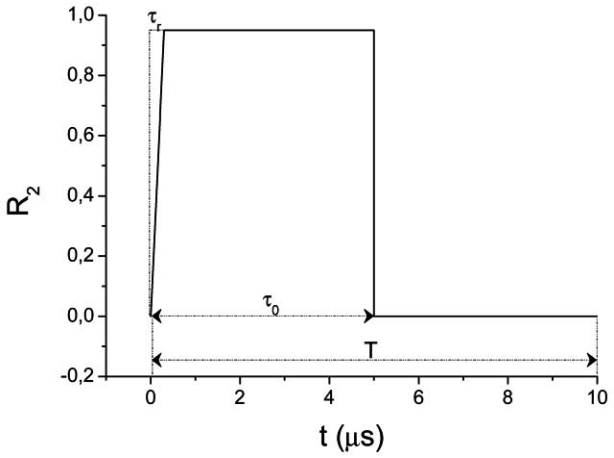

Fig. (3). Modulation of the reflectivity R_2 of the right-handed mirror.

$$R_2(t) = \begin{cases} \frac{R_2}{\tau_r} \times t, & 0 \le t < \tau_r \\ R_2, & \tau_r \le t < \tau_0 \\ 0 & t \ge \tau_0 \end{cases}$$

This modulation induces the Q-switching mechanism. At time t < 0, the pump power is applied to the laser but the acousto-optic modulator (AOM) is off. The AOM is then turned on and Q-switching can occur. In a next step, the AOM is switched off. This procedure is then repeated at a given repetition rate.

Last condition concerns the output power: P_{out}. It is obtained through:

$$P_{out}(t) = (1 - R_1) P_s^-(0,t).$$

The pulse energy is determined by:

$$E_{out}(t) = \int_{t_i}^{t} P_{out}(t)\,dt = (1 - R_1) \int_{t_i}^{t} P_s^-(0,t)\,dt .$$

where: t_i is the initial value of a time interval comprising an output pulse.

Before to present the simulations, a last point needs to be clarified: the AOM is modulated at a given repetition rate, which allows the generation of a train of pulses at this repetition rate. If this repetition rate is low (typically less than 1 kHz), the pulse that is calculated presents directly its steady state shape: all parameters have the time to return to their switch-off steady state value before a new modulation of the AOM occurs, and a second calculus of the pulse leads to a shape similar to the first one. If the repetition rate is higher, the calculated pulse reaches its steady-state shape only after 3, 4 or 5 periods of modulation (see discussion in reference [5]). In this case, the calculus of the pulse-shape is much longer as it requires many periods of modulation of the AOM until stabilization of the shape is observed. In sections 2 and 3, we consider only low-repetition rates such that the pulse-shape is calculated from a sole period of modulation. In section 4, we will consider a higher repetition rate to validate our results in all cases.

2.3. First Simulation - Validation

According to previous discussions, a model of the Q-switched double clad fiber laser has been built. The parameters used in our simulations are reported in Table **1**. The pump power W_0 is 10 W. The Ytterbium dopant concentration N_{Yb} is $4 \times 10^{25}\ m^{-3}$, and the Ytterbium-core radius R_{co} is equal to $8\ \mu m$. The right-mirror reflectivity R_2 is fixed at 95%. The length of the doped fiber is $L_{f_1} = 5\ m$. In this first case, we take $L_{f_2} = 0\ m$: there is no DSF. The fresnel reflectivity R_1 is 0.04. The rise time τ_r of the modulation is equal to $50\ ns$ and we assume $\tau_0 = 2\ \mu s$. Fig. (**4**) shows the Q-switched pulse that is predicted with the previous parameters. The pulse is calculated in the low repetition rate limit. The pulse duration is 60 ns. The most important observation is the presence of multiple peaks. This phenomenon has been already reported in references [5, 11, 12]. The separation of the neighboring peaks is actually equal to the round trip time, 47.5 ns for our 5-m fiber. When the AOM is open, the pulse formation begins. However, the reflection on the mirrors leads to the apparition of successive peaks (after each round-trip) as long as there is some gain into the amplifying medium. The global pulse is the sum of these different components.

Table 1. Parameters Used in the Simulation

Parameter	Value
σ_{ap}	3×10^{-25} (m^2)
σ_{ep}	5×10^{-26} (m^2)
σ_{as}	1.4×10^{-27} (m^2)
σ_{es}	2.5×10^{-25} (m^2)
α_p	3×10^{-3} (m^{-1})
α_s	5×10^{-3} (m^{-1})
$\Delta\lambda_s$	20 (nm)
Γ_s	0.75
h	6.626068×10^{-34} (J.s)
n	1.45
c	$3 \times 10^{+8}$ ($m.s^{-1}$)
λ_p	0.94 (μm)
λ_s	1.08 (μm)
τ_{ba}	1 (ms)

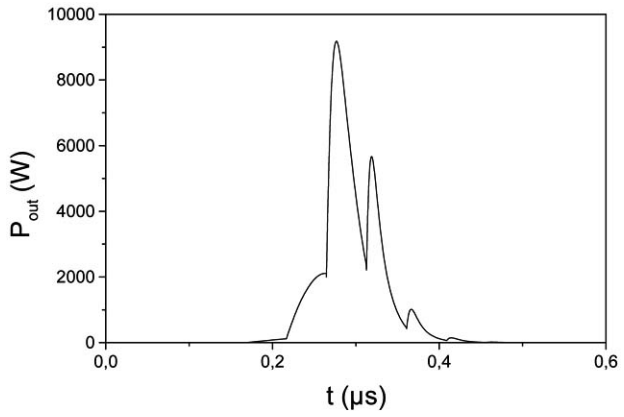

Fig. (4). Simulated output pulse.

This structure of the pulse is essential for the optimization of a bi-pulse fiber laser for PIV applications. It seems indeed possible to modify the cavity in such a way that the multiple peaks would be much more separated (more than 500 ns), that only two of them would be selected, and that an equilibrium of the energy repartition between them would be realized.

- In order to separate the multiple peaks, it seems indeed possible to use a longer fiber. Unfortunately, the use of a longer amplifying fiber would generate multiple peaks much more separated, but each of them being much longer. In our case, each peak must conserve a pulse duration of approximately 10 ns. This is why we will consider a configuration with two different fibers: the amplyfing Yb-doped fiber which will generate the pulse composed of multiple peaks, and an undoped fiber (which can be spliced on the right hand side of the previous fiber): This latter fiber will lead to an enhancement of the separation between the multiple peaks, but will not contribute to increase their respective pulse durations.

- The selection of only two peaks should be easily obtained by adjusting the switching open time τ_0 of the AOM.

- The equilibrium between the two pulses, in terms of energy, should be obtained by an appropriate adjustment of two parameters: the reflectivity coefficient R_1 and the rise time τ_r.

Next section will present the main results of our optimization.

3. FIBER LASER OPTIMIZATION FOR PIV APPLICATIONS

As previously mentioned, the lengths of the fibers have to be optimized to adjust the separation between the multiple peaks, and parameters τ_0, τ_r and R_1 have to be selected to select two similar peaks. Let us detail some steps of this optimization process.

We show first in Fig. (**5**) the influence of the lengths of the two fibers. The different parameters are unchanged: $W_0 = 10$ W, $N_{Yb} = 4\times10^{25}\ m^{-3}$, $R_{co} = 8$ µm, $R_1 = 0.04$, $\tau_0 = 2$ µs and $\tau_r = 50$ ns. The sole differences are the fiber lengths. We choose in this case: $L_{f_1} = L_{f_2} = 10\ m$. Fig. (**5**) presents the pulse shape obtained in this case. The round-trip time τ_{rt} of the corresponding cavity is 193 ns. We can observe well-separated pulses. The energy of the two first peaks is 0.97 mJ and 0.52 mJ while their respective durations are 39 ns and 9 ns. The temporal spacing between the peaks is 193 ns, which corresponds to the theoretical round-trip time. These results confirm that the temporal interval between the successive pulses is widened when the fiber length is increased. The shape of the different peaks is however very different (pulse durations and energies) and a further optimization step is required.

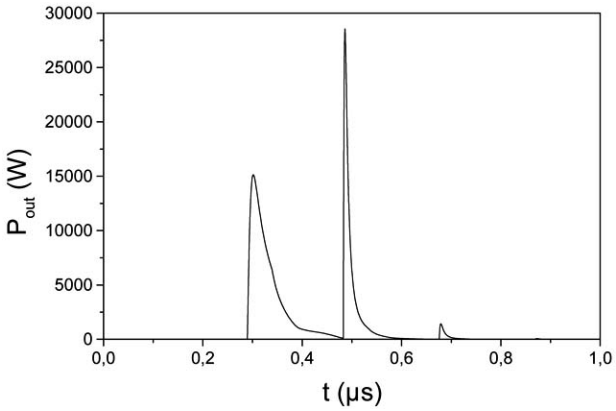

Fig. (5). Output pulse with a total fiber length of 20 m and a 50-ns rise time.

The rise time τ_r of the modulation is another very important parameter. Fig. (**6**) shows the Q-switched pulses that are predicted for a different rise time $\tau_r = 5.5$ ns. The other parameters are unchanged: $W_0 = 10$ W, $N_{Yb} = 4\times10^{25}\ m^{-3}$, $R_{co} = 8$ µm, $R_1 = 0.04$, $\tau_0 = 2$ µs and $L_{f_1} = L_{f_2} = 10\ m$. We observe the emission of pulses composed of multiple peaks. The temporal interval between successive peaks is still 193 ns. The energy and the full-width at half-maximum (FWHM) of the different peaks are (1.03 mJ; 8 ns) and (0.44 mJ; 5 ns) respectively. It can be observed that the peak duration at FWHM diminishes when the rise time τ_r increases. A very fast switching produces indeed a sharp amplified spontaneous emission (ASE) pulse (as described in Ref. [5, 12, 13]) which travels around the cavity, being amplified periodically during each round-trip. On the other hand, a slow switching delays the buildup of the pulse, and decreases the output peak power. Note that the influence of τ_r on laser output would be more significant for a smaller fiber core, because the ASE buildup time would be faster in this case [14]. In conclusion of this step, the rise time remains a very important factor in our study. We can see from Fig. (**6**) that the emission of two similar pulses is possible by mastering the rise time of switching. Note that it is however not sufficient for PIV applications which require the emission of pulses separated by more than 500 ns. In addition, both pulses are not rigorously identical and further optimization is required.

These previous calculations show that the rise time and the fiber length are two important factors which influence

the output pulse shape. It seems thus possible to produce a pair of pulses largely separated and exhibiting the same energy.

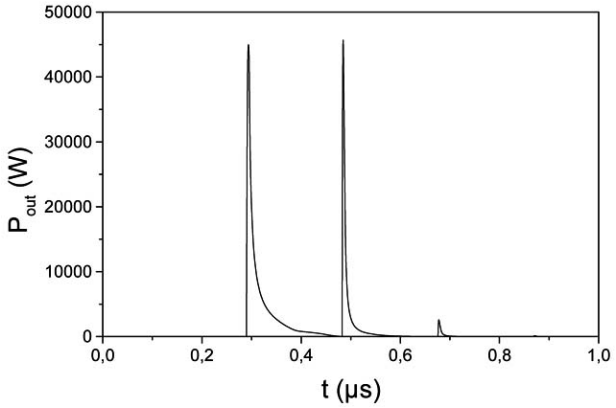

Fig. (6). Output pulse with a total fiber length of 20 m and a 5.5 ns rise time.

4. OPTIMIZED BI-PULSE FIBER LASER

Based on previous observations, we have repeated our calculation of pulse shapes with different cavity lengths, AOM rise time to design a Q-switched bi-pulse fiber laser for PIV application (i.e. a laser that can emit two pulses with the following characteristics: identical energy, pulse width of approximately 10 ns, time interval between the pulses of more than 500 ns).

Considering the previous conclusions, and to separate two pulses by a time upper of 500 ns, we take two fiber lengths: $L_{f_1} = 25\ m$ and $L_{f_2} = 40\ m$ (the theoretical round-trip time τ_{rt} of the corresponding cavity is approximately 628 ns). As the doped-fiber is longer than in previous case, the ion doping concentration is slightly reduced to 1.45×10^{25} m^{-3}. The switching open time τ_0 equals 1.9 ns. The other parameters are unchanged: R_{co} = 8 µm, $R_1 = 0.04$ and τ_r = 5.5 ns. The pump power is 10.75 W. Fig. (**7**) shows the pulse obtained in this case. We obtain two pulses exhibiting approximately identical peak powers of 22.75 and 19.86 kW respectively, and separated by approximately 626 ns. The round-trip time of the cavity is 626 ns. The full-width at half-maximum of the output pulses are 11.6 ns and 7.5 ns respectively. The energies of both pulses are however very different: 0.74 mJ and 0.27 mJ. A last parameter can be actually used to equilibrate the two pulses energetically: the left hand-side reflectivity R_1.

Finally, we consider the following set of parameters: W_0 = 10.75 W, $N_{Yb} = 1.45 \times 10^{25}$ m^{-3}, R_{co} = 8 µm, $R_1 = 0.95$, τ_0 = 1.9 µs, $L_{f_1} = 25\ m$, and $L_{f_2} = 40\ m$. Fig. (**8**) shows the pulses generated in this case. Two cases are considered: the low repetition modulation limit (Fig. **8a**), and a 42 kHz repetition rate (Fig. **8b**). In this last case, the steady-state pulse shape is obtained after 5 periods of the AOM modulation (see our previous comment). For comparison, the steady-state pulse shape in the low repetition rate limit is obtained directly.

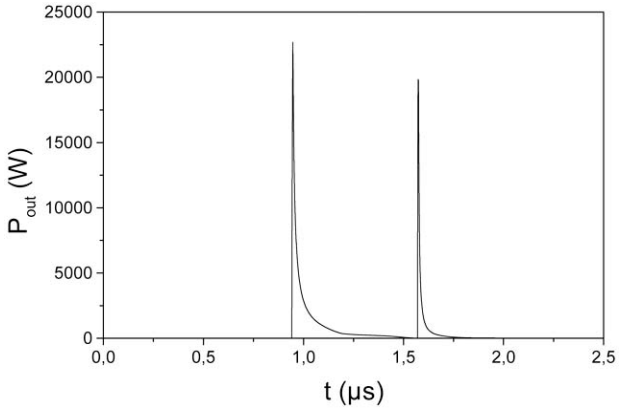

Fig. (7). Output pulse with a total fiber length of 65 m, a 5.5 ns rise time, and a reflectivity R_1 of 4%.

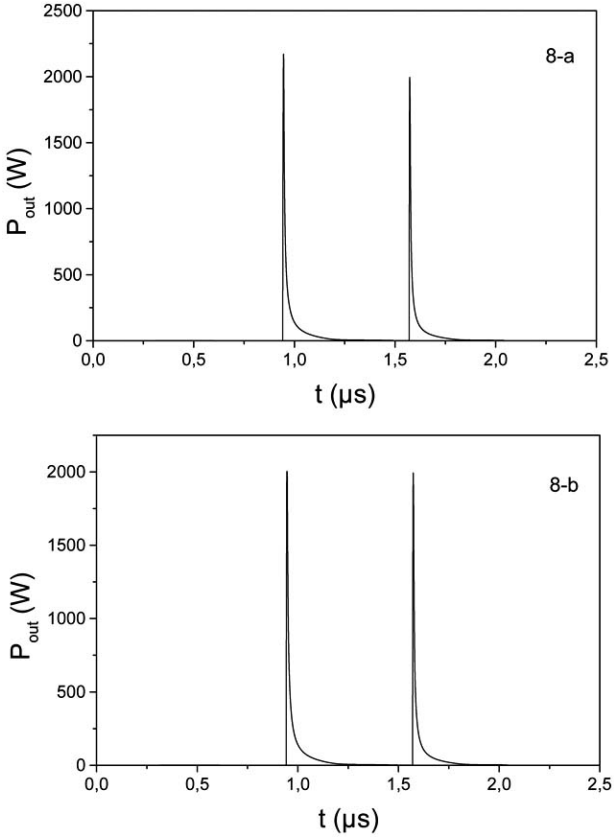

Fig. (8). Output pulse with a total fiber length of 65 m, a 5.5 ns rise time, and a reflectivity R_1 of 95% in the low repetition-rate limit (**8-a**) and at 42 kHz repetition rate (**8-b**).

In the low repetition rate limit, the energies of the two pulses are 40 µJ and 33 µJ while their pulse-durations at FWHM are 8.46 ns and 7.25 ns respectively. The temporal spacing between the two pulses is equal to 626 ns. This value is approximately equal to the 628-ns theoretical round-trip time of our 65-m linear cavity.

With a 42 kHz repetition rate, the energies of the two pulses are 36.5 µJ and 35 µJ while their pulse-durations at FWHM are 8.15 ns and 8.1 ns respectively. The temporal

spacing between the two pulses is equal to 626 ns. In conclusion, we have designed a cavity that is able to generate two nanosecond pulses with either a low, or a high repetition rate.

To better understand this behavior, we present in Fig. (**9a-c**) the formation of the two pulses within the cavity:

- Fig. (**9a**) shows the P_s^- profile (in blue) and the N_b profile (in black) along the fiber at time t_a = 940 ns (the time origin t = 0 corresponds to the opening of the AOM). We observe the first pulse just before leaving the cavity (by the left). The pulse formation is accompanied by an abrupt decrease of the N_b population.
- Fig. (**9b**) shows then the P_s^+ profile (in blue) and the N_b profile (in black) along the fiber at time t_b =1050 ns (the first pulse is already out). We observe now the formation of the second pulse. It is still accompanied by an abrupt decrease of the N_b population still available.
- Fig. (**9c**) shows finally the P_s^- profile (in blue) and the N_b profile (in black) along the fiber at time t_c =1550 ns, just before leaving the cavity (by the left). This is the end of the formation of the second pulse. Its formation is accompanied by decrease of the N_b population still available.

In conclusion, we have designed a cavity that is able to generate two nanosecond pulses with either a low, or a high repetition rate. These data confirm that it should be possible to replace the usual Nd:YAG bi-pulse laser sources by compact, low-cost fiber lasers in PIV applications.

5. CONCLUSION

We have presented in this article the design of a fiber laser cavity that is able to emit a pair of pulses separated by more than 500 ns. The energy per pulse exceeds some tens of microjoules, and such a laser would satisfy PIV requirements. This offers an important domain of applications to compact, low cost, fiber lasers. In addition, such a device would significantly improve the precision in PIV experiments because the spatial alignement of the two pulses would be systematically realized (Both pulses are emitted by the same single-mode fiber).

APPENDIX

The evolution of the laser level populations is described by the following rate equations [8]:

$$\frac{\partial N_b(y,t)}{\partial t} = \left[R_{ab}(y,t) + W_a(y,t)\right] N_{Yb} - \left[R_{ab}(y,t) + R_{ba}(y,t) + W_a(y,t) + W_e(y,t) + A_{ba}\right] N_b(y,t), \quad (1.a)$$

and

$$N_a(y,t) = N_{Yb} - N_b(y,t), \quad (1.b)$$

where N_{Yb} is the total Yb dopant concentration which is assumed to be uniform along the fiber. The transition rates are equal to:

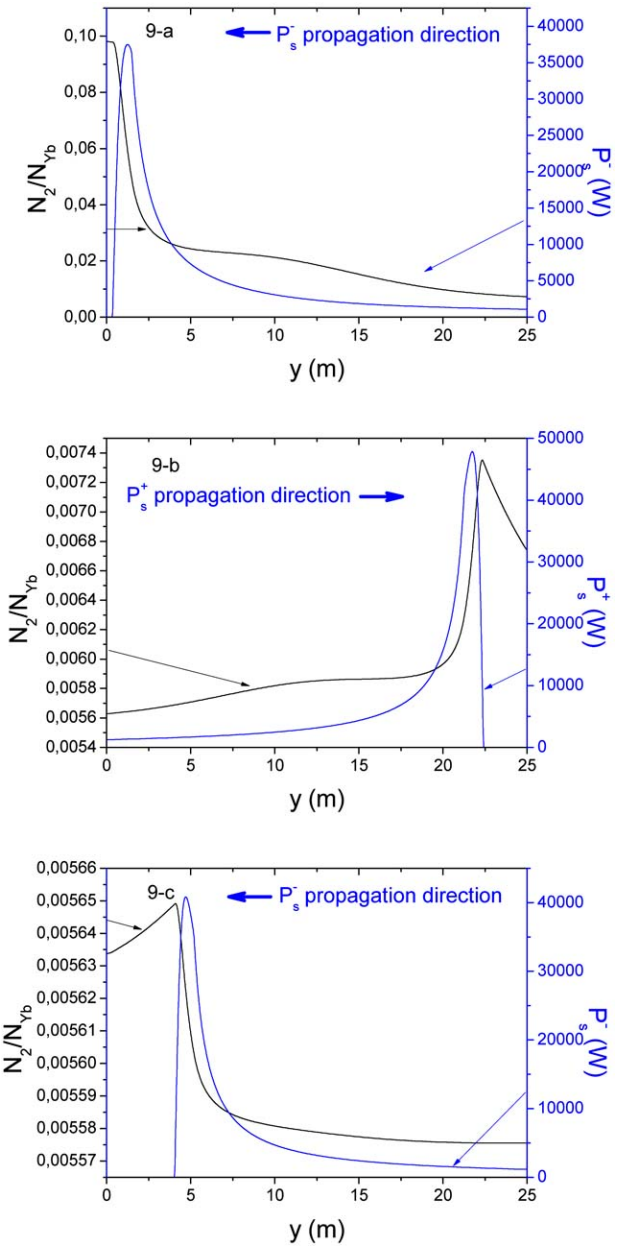

Fig. (9). evolution of P_s^- (P_s^+ at time t = 1050 ns) and of the N_2 population along the fiber at different times after the opening time of the acousto-optic modulator: 940 ns (**9-a**), 1050 ns (**9-b**), and 1550 ns (**9-c**).

$$R_{ab}(y,t) = \frac{\sigma_a(\lambda_p) P_p(y,t) \Gamma_p}{A_{co} h \upsilon_p}, \quad (2.a)$$

$$R_{ba}(y,t) = \frac{\sigma_e(\lambda_p) P_p(y,t) \Gamma_p}{A_{co} h \upsilon_p}, \quad (2.b)$$

$$W_a(y,t) = \frac{\sigma_a(\lambda_s) \left[P_s^+(y,t) + P_s^-(y,t) \right] \Gamma_s}{A_{co} h \upsilon_s}, \quad (2.c)$$

$$W_e(y,t) = \frac{\sigma_e(\lambda_s) \left[P_s^+(y,t) + P_s^-(y,t) \right] \Gamma_s}{A_{co} h \upsilon_s}, \quad (2.d)$$

where $\sigma_a(\lambda_p)$ and $\sigma_e(\lambda_p)$ are the absorption and emission cross sections for the pump respectively; and $\sigma_a(\lambda_s)$ and $\sigma_e(\lambda_s)$ are the absorption and emission cross sections for the signal, respectively. The absorption and stimulated emission rates between levels (a) and (b) are denoted respectively by W_a and W_e. The radiative and non-radiative relaxation rates from level (b) are called respectively A_{baR} and A_{baNR}. As the relaxation is essentially radiative, A_{baNR} is neglected in front of A_{baR}, which is noted simply $A_{ba} = \frac{1}{\tau_{ba}}$.

A_{co} is the core area. The fraction of the pump power actually coupled into the active core is represented by the power filling factor Γ_p given approximately by the ratio between the area of the core and that of the first cladding. Γ_s is the power filling factor describing the fraction of the signal amplified in the core. υ_p and υ_s are pump and signal frequencies, The propagation equations in the Yb-doped fiber for the pump and signal lights are written as

$$\frac{\partial P_p(y,t)}{\partial y} + \frac{1}{v}\frac{\partial P_p(y,t)}{\partial t} = \Gamma_p\left[\left(\sigma_a(\lambda_p)+\sigma_e(\lambda_p)\right)N_b(y,t) - \sigma_a(\lambda_p)N_{Yb}\right]P_p(y,t) - \alpha_p P_p(y,t), \quad (3.a)$$

$$\pm\frac{\partial P_s^{\pm}(y,t)}{\partial y} + \frac{1}{v}\frac{\partial P_s^{\pm}(y,t)}{\partial t} = -\Gamma_s\left[\sigma_a(\lambda_s)N_{Yb} - \left(\sigma_a(\lambda_s)+\sigma_e(\lambda_s)\right)N_b(y,t)\right]P_s^{\pm}(y,t) + 2\Gamma_s\sigma_e(\lambda_s)n_m hc^2\frac{\Delta\lambda_s}{\lambda_s^3}N_b(y,t) - \alpha_s P_s^{\pm}(y,t), \quad (3.b)$$

In the above equations, $v = \frac{c}{n}$ is the velocity of light propagation in the active medium, c is the velocity of light in vacuum, n is the refractive index, and α_p and α_s are the pump and signal loss factors, n_m is the number of modes, and $\Delta\lambda_s$ is the signal bandwidth.

Let us now detail the behavior in the undoped fiber (a dispersion-shifted single-mode fiber (DSF) in our case, see Fig. **1**). The attenuation of pump and signal in the DSF can be neglected as the fiber length will not exceed 100 m [12] and the attenuation constants of the DSF are sufficiently small. The propagation of light in this fiber can thus be simply written:

$$\frac{\partial P_p(y,t)}{\partial y} + \frac{1}{v}\frac{\partial P_p(y,t)}{\partial t} = 0, \quad (4.a)$$

$$\pm\frac{\partial P_s^{\pm}(y,t)}{\partial y} + \frac{1}{v}\frac{\partial P_s^{\pm}(y,t)}{\partial t} = 0, \quad (4.b)$$

Continuity between the doped and undoped fibers is ensured with appropriate boundary conditions.

We integrate Equations (1)-(3) and (5) by Explicit Euler Method. The position and time steps integration Δy and Δt respectively are related by $\Delta t = \frac{\Delta y}{v}$. Thus, by dividing the fiber into equally segments (200 segments for a case of 5m-length fiber [5]) of smallest Δy according to the length fiber, we can obtain accurate results. The time development of the system is given in [5]. Continuity is ensured at the boundary of the fiber.

ACKNOWLEDGEMENT

M. Brunel wishes to thank Agence Nationale de la Recherche (program VIVE3D) for financial support.

REFERENCES

[1] Adrian RJ. Scattering particle characteristics and their effect on pulsed laser measurements of fluid-flow – speckle velocimetry vs particle image velocimetry. Appl Opt 1984; 23: 1690-1.

[2] Willert CE, Gharib M. Digital particle image velocimetry. Exp in Fluids 1991; 10: 181-3.

[3] Hideur A, Chartier T, Brunel M, et al.. Mode-lock, Q-switch and CW operation of an Yb-doped double clad fiber ring laser . Opt Commun 2001; 198: 141-6.

[4] Ortac B, Hideur A, Brunel, M. Passive harmonic mode-locking with a high-power Yb-doped double-clad fiber laser. Opt Lett 2004; 29: 1995-7.

[5] Huo Y, Brown RT, King GG, Cheo PK. Kinetic modeling of Q-switched high-power ytterbium-doped fiber lasers. Appl Opt 2004; 43: 1404-11.

[6] Selvas R, Torrez-Gomez I, Martinez-Rios A, et al. Wavelength tuning of fiber lasers using multimode interference effects. Opt Exp 2005; 13: 9439-45.

[7] Gaeta CJ, Digonnet MJF, Shaw HJ. Pulse characteristics of Q-switched fiber lasers. J Lightwave Technol 1987; LT-5: 1645.

[8] Morkel PR, Jedrzejewski KO, Taylor ER. Q-switched neodymium-doped phosphate glass fiber lasers. IEEE J Quantum Electron 1993 ; 29: 2178.

[9] Stone DH. Effects of axial nonuniformity in modeling Q-switched lasers. IEEE J Quantum Electron 1992; 28: 1970.

[10] Roy P, Pagnoux D. Analysis and optimization of a Q-switched Erbium-doped fiber laser working with a short rise time modulator. Opt Fiber Technol 1996; 2: 235-40.

[11] Wang Y, Martinez-Rios A, Po H. Analysis of a Q-switched ytterbium-doped double-clad fiber laser with simultaneous mode locking. Opt Commun 2003; 224: 113-23.

[12] Adachi S, Koyamada Y. Analysis and design of Q-switched erbium-doped fiber lasers and their application to OTDR. J Lightwave Technol 2002; 20: 1506-11.

[13] Myslinski P, Chrostowski J. High power Q-switched Erbium doped fiber laser. IEEE J Quantum Electron 1992; 28: 371-7.

[14] Wang Y, Xu CQ. Modeling and optimization of Q-switched double-clad fiber lasers. Appl Opt 2006; 45: 2058-71.

Received: June 5, 2009 Revised: July 30, 2009 Accepted: August 20, 2009